Journal of Ultrafine Grained and Nanostructured Materials
https://jufgnsm.ut.ac.ir
Vol. 58, No.2, June 2025, pp. 228-241
Print ISSN: 2423-6845 Online ISSN: 2423-6837
DOI: 10.22059/jufgnsm.2025.02.08

Development of Valve Steel containing of a Blend of Hard Phases for High-Temperature Applications

Taher El-Bitar[1], Maha El-Meligy[1,*], Mohammed Gamil[2]

[1]Plastic Deformation Department, Central Metallurgical R&D Institute (CMRDI), Cairo 11422, Egypt
[2]Department of Mechanical Engineering, Faculty of Engineering at Shoubra, Benha University, Cairo 11629, Egypt

Recieved: 31 July 2025; Accepted: 6 November 2025

[*]Corresponding author, E-mail: dr.mahaelmeligy@gmail.com

ABSTRACT

A steel alloy was developed containing 0.36 wt % Carbon coexisting with 9.15 wt % chrome, 2.44 wt % silicon and 0.986 wt % molybdenum. Multi-directional hot forging was implemented on 5 successive steps, for grains refinement with homogeneously distributed embedded Cr/Mo carbides. Forging at the 1st step was carried out at 1150 °C and finished at 1000 °C, while the final 5th deformation step was finished at 890 °C, where the cross-section area reduction was reaching to 64.03 %. The Z-parameter was then evaluated for each forging step. It is found that the Z-parameter increases continuously, which is resulting in successive decrease of expected γ-grain size, and consequently the generated microstructure is subjected to repeated grain refinements. The forged steel rods were then heat treated at 930 °C and soaked for 15 min. and followed by a salt bath 1st quenching at 400 °C for 15 min. And followed by oil (2nd) quenching. After the 2nd quenching cycles, the generated microstructure contains bainite islands interspersing across freckled ferrite matrix with scattered Cr/Mo carbides. The generated bainite is featured with a low carbon content. Thermodynamically, Cr/ Mo carbides are the most stable carbides within the working temperature range. The bainitic aggregates are found surrounded by thin retained austenite films. Quenching in water after salt bath treatment creates platelet late martensite integrated with the widespread Cr/Mo carbides, that existing between the ferrite matrix grains.

Keywords: *Valve steel, Multi-directional hot forging, Cr-Mo carbides, Bainite generation, Retained austenite, Late martensite. Salt bath, Oil and water quenching.*

1. Introduction

Steel alloys for hot temperature service contains considerable amounts of Mo, where Mo suppresses the carbide coagulation at the hot temperature environment for a long time. Improper alloying with Mo leads to decay of the steel by coagulated carbide formations at the grain boundaries and triple points, accelerating the creep rate [1]. Coagulated carbide formations are considered as an easy path for micro-cracks initiation during the hot temperature working conditions due to a combination of mechanical and thermal fatigue [2]. Micro-cracks would further lead to formation of fatigue failure at stresses below the yield point of the material [3]. On the other hand, Cr alloying provides high oxidation resistance and raises alloy hardening ability, while Si besides Cr are working to together to secure a ferrite phase matrix at room temperature and up to Ac1 temperature [4].

Thermodynamic calculations and phase thermal analysis on the hot temperature service steel containing Cr and Mo ensured formation of strong-stable carbides containing $Cr_{23}C_6$ and Mo_2C at 350 °C as a working temperature.

Thermodynamically, $Cr_{23}C_6$ shows the most negative Gibbs free energy change of formation (-ve ΔGo), indicating the high stability among the others [4-6]. A Finite Element simulation explained that carbides could be precipitated in the form of band, net, random and cluster structures, where cracks propagate in the net-like carbide following the carbide network [7,8].

On heating valve steel to a temperature higher than Ac_1 during forging, a portion of the ferrite matrix is transformed to austenite phase and the cluster carbides are then dissolute, where some carbon transfer to austenite and carbides become thinner with smaller sizes [4]. A fracture surface investigation of a failed exhaust valve showed ferrite facets matrix coexisting with embedded cluster carbides causing a thermal yielding [1, 2].

High strength of valve steel, in the hot temperature environment needs for strong and stable carbide forming elements like Cr and Mo besides Carbon [9, 10]. Fig. 1 presents the free energy for carbides formation. It is clear that $Cr_{23}C_6$ is the most stable carbide during the whole working temperature range (up to 350 °C). Furthermore, Mo_2C still stable at temperatures near 700 °C [4, 6]. Furthermore, Mo plays another essential role that serve in suppressing the carbides coagulation in the valve alloy during working in the hot temperature environment. Consequently, Mo deficiency in the alloy content would result in a decay of mechanical properties [9]. i.e. alloying with Cr and Mo is essential for strength stability during working in hot environment.

In valve steel for hot working service, a post heat treatment process is essential for generation of hard-stable phases like martensite and/or bainite. Salt baths are appropriate for quenching from the austentizing temperature to hard phase start temperature [11]. Isothermal holding time at the phase start temperature is a must, especially for bainite phase generation [12], while creation of martensite does not need for the holding time at the salt bath. Recently, investigations have been executed for the nature of bainite phase generation and detection of accompanied phases in different alloys [13]. It is found that a steel alloy held in a salt bath at 420 °C, bainite aggregates has been generated and integrated with some martensite/ retained austenite phases after cooling to the room temperature [13]. The bainitic aggregates are composed of bainitic ferrite laths and retained austenite films [12, 13]. Retained austenite is originating from a residual austenite that is un-transformed into bainite at the end of isothermal holding but partially transforms during subsequent cooling into ferrite and late martensite because of its low thermal stability [13].

A schematic presentation of the microstructure changes during austenitizing [14], before hot forging processes, is demonstrated in Fig. 2. Heating continues to above the critical temperatures (Ac_1 and Ac_3), where the as cast microstructure exhibits coarse ferrite grains due to slow rate of cooling during solidification in the sand mold [9]. Furthermore, majority of carbides are precipitated as clusters scattered and integrated with the ferrite grains [9]. On heating to Ac_1 temperature, the ferrite (α) phase starts to transform gradually to the austenite (γ) forming a blend of α+γ phases. Further increase of the heating temperature up to Ac_3, the matrix is transformed completely to austenite (γ) phase [4] and the scattered cluster carbides are dissolute to reach a finer size [9]. The Ac_1 temperature was calculated by the software (JMatPro) as 873 °C while the Ac_3 was calculated as 914 °C [4].

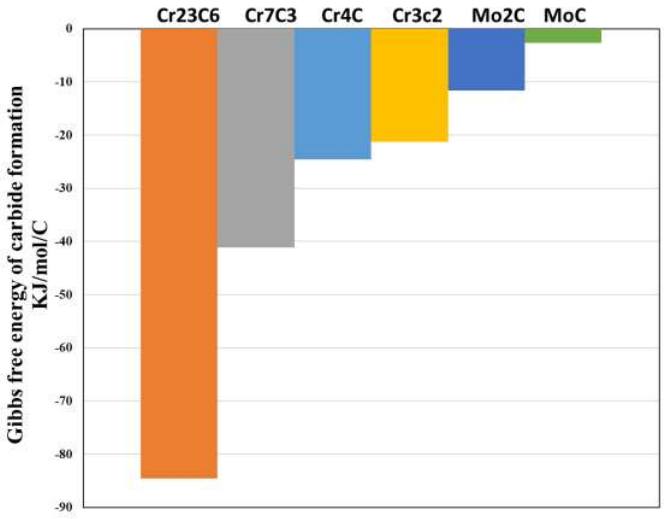

Fig. 1- Gibbs free energy for Cr and Mo carbides stability or formation at 350 °C [4, 6].

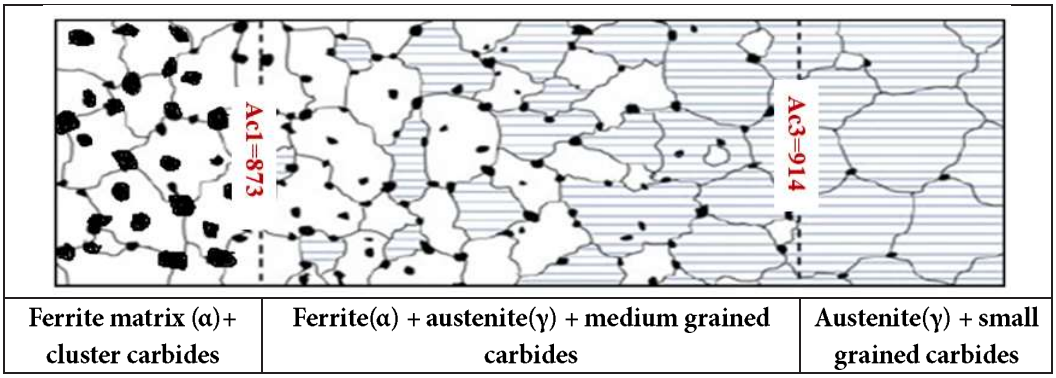

Fig. 2- A schematic presentation of microstructure changes during austenitizing, before hot forging processes [14].

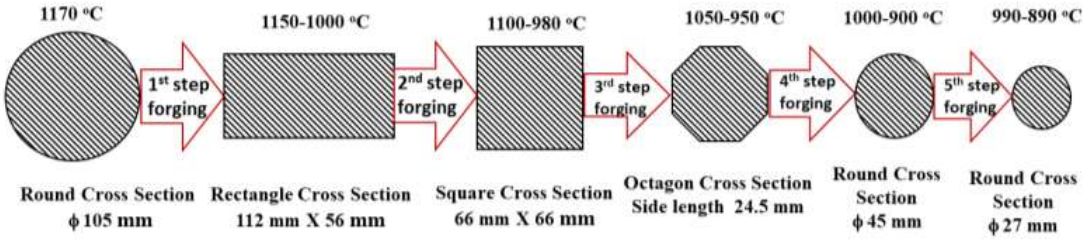

Fig. 3- Demonstration of 5-step hot forging cycles.

2. Experimental Work

A steel alloy was developed containing 0.36 wt % Carbon coexisting with 9.15 wt % chrome, 2.44 wt % silicon and 0.986 wt % molybdenum. Melting and casting details and microstructure investigation of the cast alloys were published through the Metal Forming conference 2024, Materials Research Forum LLC [9].

The as-cast steel ingots were subjected to 5-step hot forging cycles, as demonstrated in Fig. 3. including changes in dimensional cross-sectional shapes, start and finish temperature of each step.

The forging process was starting by heating for austenitizing the ingots to 1200 °C and followed by holding for 8 min to secure fully austenite phase having and dissolution of carbides before forging, Fig. 4. At the 1st step, the 105 mm round diameter ingots were deformed by 27.5% area reduction forming rectangles with cross sections 112x56 mm^2. At the 2nd step, the rectangle cross sections were forged to squares with 66 mm edges subjecting to 30.55% area reduction. At the 3rd step the squares are deformed into octagons with side lengths 24.5 mm, with cross section area reduction 33.47%. The last 2 steps, were carried out with the same manner to the 5th finishing step resulting in 27 mm round diameter bars at a final temperature 890 °C.

It was difficult to accept unrealistic allotropic bainite transformation temperature range (Bs and Bf) provided by a software package for the current steel alloy [4]. A controlled cooling curve was constructed by a thermo-mechanical simulator (Gleeble 3800) with 5 °C/sec average cooling rate as stated in Fig. 5, for exploration and detection of the bainite transformation range.

Fig. 6 demonstrates the dilation curve, which contains deflections confirming bainite transformation between 380 °C and 460 °C.

Consequently, a heat treatment cycle was constructed for bainite as well as martensite generation by double quenching technique. Fig. 7 demonstrates the double quenching technique by heating to 930 °C for austentizing and holding for 15 min. The austentized samples are then quenched in a salt bath at 400 °C and held for 15 min for bainite formation, and followed by quenching in either oil or water for martensite formation from the rest of austenite.

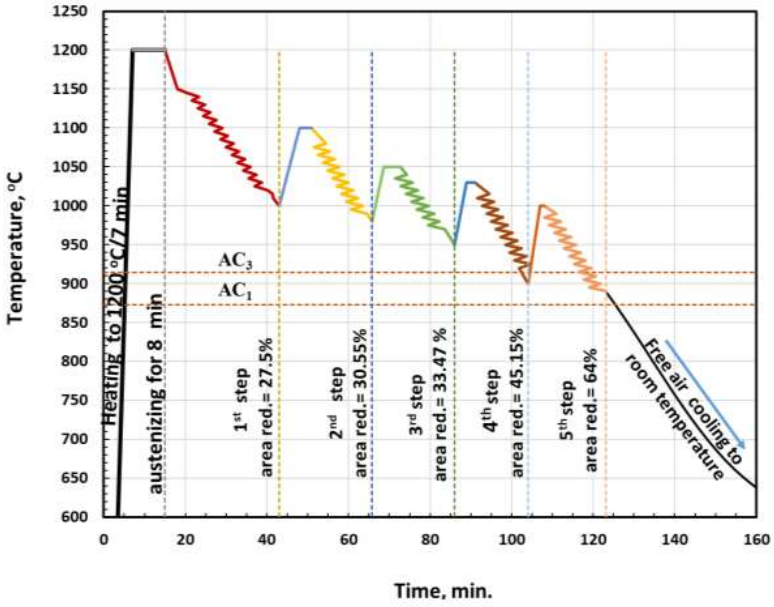

Fig. 4- Forging temperature and cross-sectional area reduction for each of the 5 steps hot deformation.

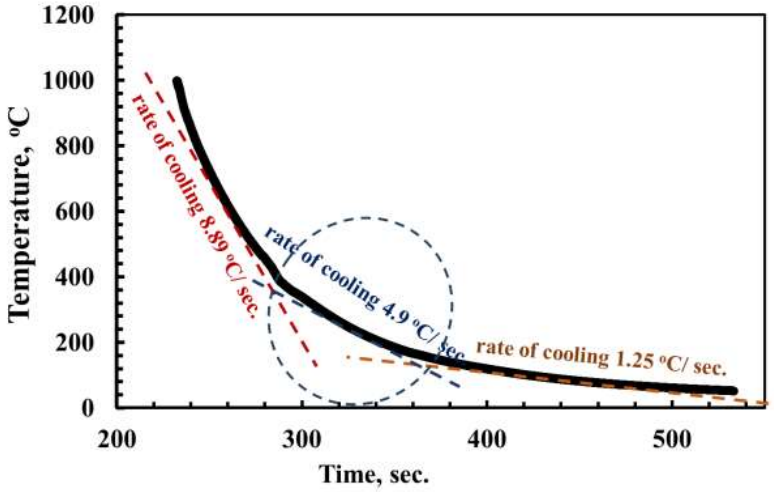

Fig. 5- A controlled cooling curve constructed with average cooling rate 5 °C/sec.

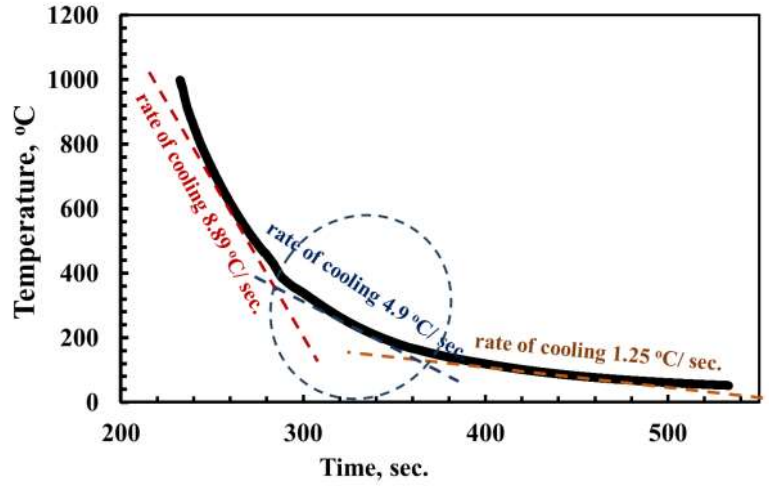

Fig. 6- Dilation curve, containing deflections confirming bainite transformation range between 380 and 460 °C.

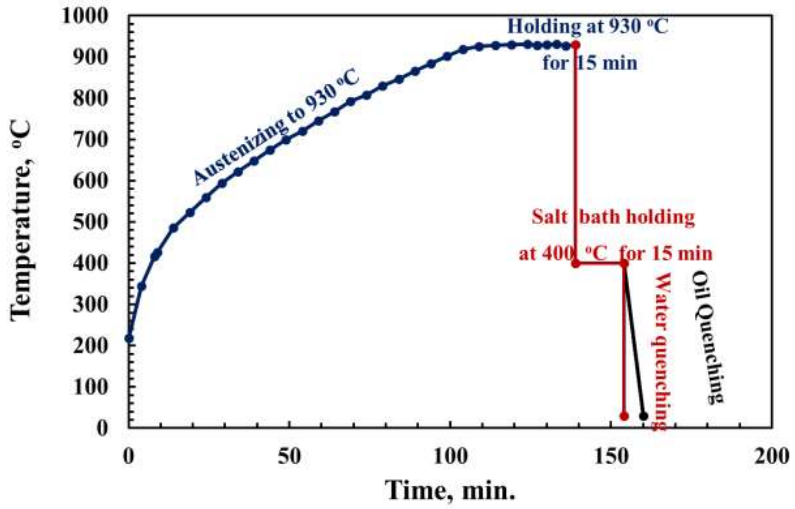

Fig. 7- Heat treatment cycle demonstrating austentising at 930 °C followed by salt bath 1st quenching at 400 °C for 15 min and then 2nd quenching either in oil or in water.

Further investigation of microstructure was carried on the double quenching samples. A scanning electron microscope (SEM) was additionally used for high magnification and EDX qualitative analysis.

3. Results and discussion

Fig. 8 demonstrates amount of phase transformations by continuous heating. The Figure confirms existence of both rich Cr-carbides as $Cr_{23}C_6$ up to 960 °C and rich Mo-carbides as Mo_2C up to 1000 °C [4,14].

Forged microstructure at magnification 4000X by the SEM is presented in Fig. 9. It emphasizes that the matrix composes mainly of ferrite grains as a result of air cooling after forging [9]. The ferrite matrix grains are enveloped by a thin carbide layer.

Fig 10 presents cooling after forging, where the steel undergoes to the critical transformation from γ- phase to the γ+α bi-phases with precipitated scattered carbides [4, 9]. Some of the carbides are precipitated over α-grain surface (A), while other carbides are trapped between the α-grain boundaries, showing sizes variation between 600 nm and 1.16 μm as presented in (B).

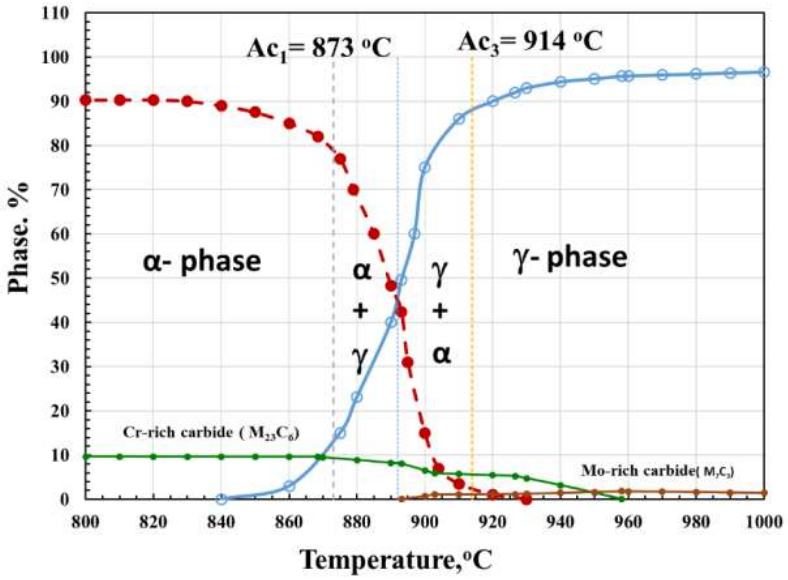

Fig. 8- amount of phase changes and existence of stable Cr- and Mo-carbides by continuous heating.

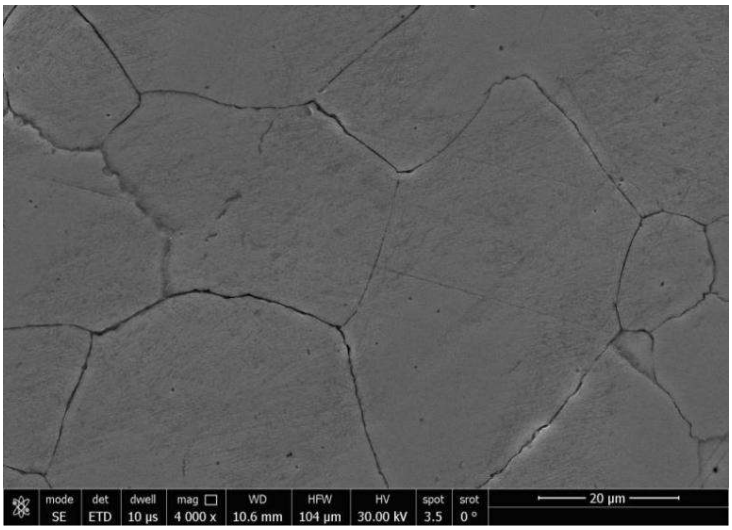

Fig. 9- Ferrite matrix grains enveloped by a thin carbide layer after 5 steps multi-directional hot forging.

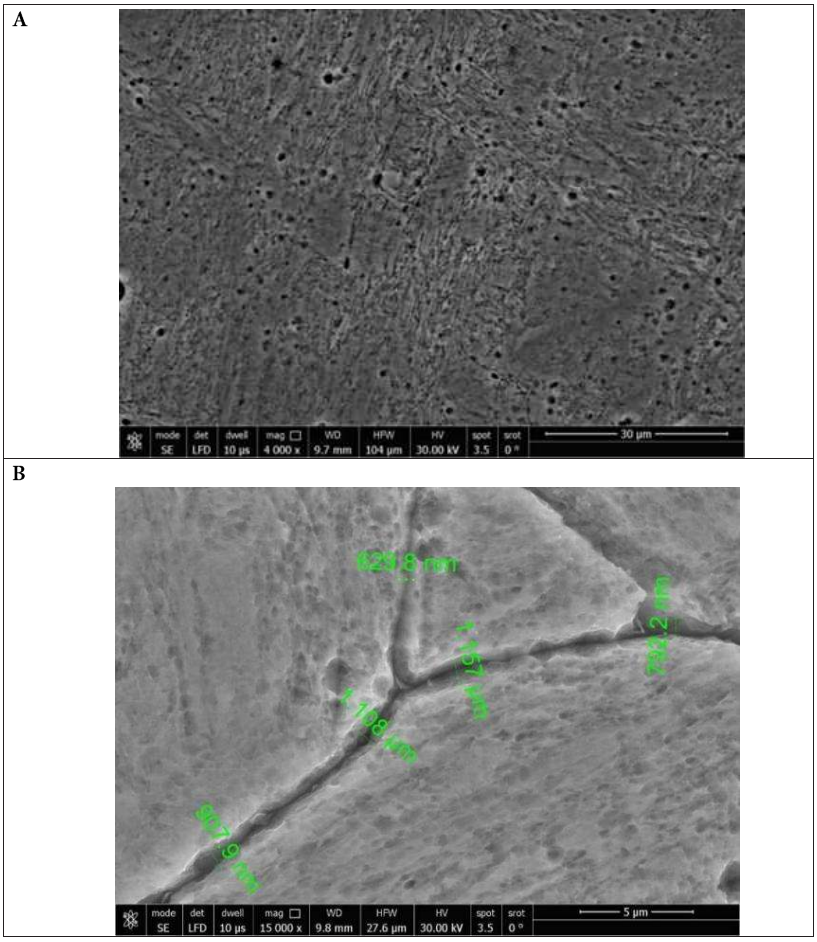

Fig. 10- Microstructure showing carbide precipitates during cooling after forging.
A- Carbides precipitated over α-grain surface, B - Carbides trapped between the α-grain boundaries.

The trapped carbides have a friable nature that facilitating to get away of the surface. These carbides are mainly Cr-Mo carbides [4], which are confirmed by the energy dispersive x-ray (EDX) qualitative an analysis at Fig. 11. It is found that some of the γ- grains, on cooling, are transformed to early martensite colonies (aggregates). Selected points on the surface of the steel alloy after forging was qualitative analyzed by the Energy dispersive x-ray (EDX) analysis. Most of precipitated carbides envelope the ferrite grains and intersect at the ferrite triple points. However, some of carbides are fine and dispersed distributing over the α-grains, as presented in Fig. 11.

Fig. 12 demonstrates numerous measurements which are taken on different grain diameters of the forged microstructure (A). A statistical assessment of grain size distribution of the ferrite matrix is presented in (B). The average measured grain size was calculated as 32 µm with a Standard deviation 12.11.

Z-parameter, for each forging step, is numerically calculated, by following equation [15]:

$$\text{Z-parameter} = \varepsilon \cdot e^{Q/RT} \quad (1)$$

Where;

ε: strain rate, s^{-1}.

Q : activation energy for deformation and equals 366.105 kJ/mol [16,17].

R : universal gas constant and equals 8.314 J/mol.K

T : absolute temperature, K

Consequently, the numerical calculation of austenite grain size (D_A) is then calculated as; $D_A = 319.81202 - 13.6114\, lnZ + 0.15322(lnZ)^2, \mu m$ [18].

Different forging parameters are then tabulated in table I.

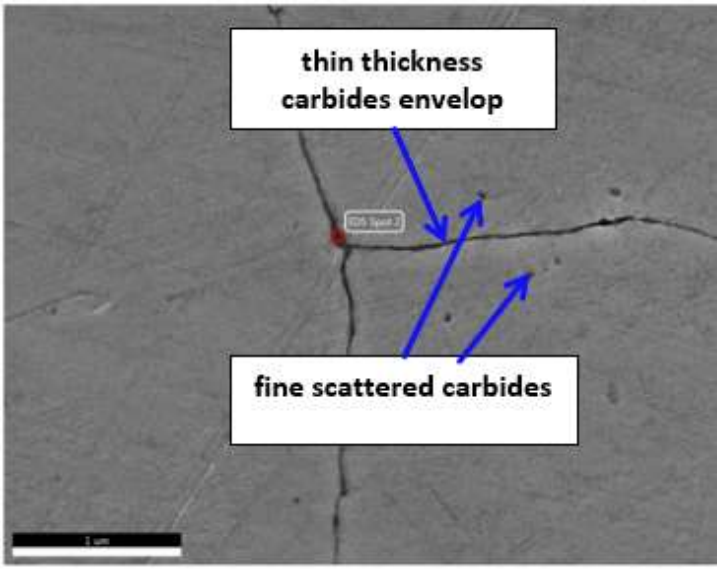

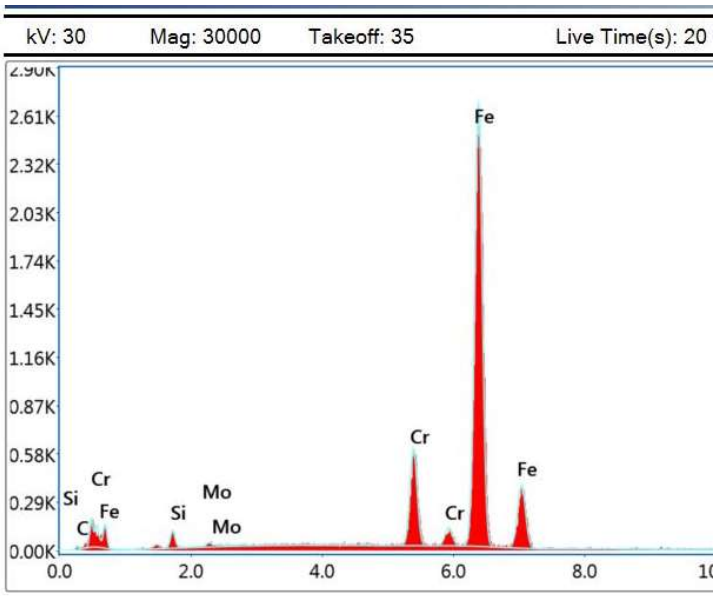

Smart Quant Results

Element	Weight %	Atomic %	Error %
C K	2.3	9.86	21.57
SiK	2.16	3.95	13.7
CrK	12.07	11.95	3.32
FeK	76.46	70.48	1.96
MoK	7	3.76	41.12

Fig. 11- EDX qualitative analysis of thin layered Cr and Mo carbides enveloping around the ferrite grains and fine scattered carbides spreading over the ferrite grains.

Table. 1- Different parameters calculated for 5 steps forging cycle

Pass #	Initial cross-section area, mm^2	Cross-section area after pass, mm^2	Strain, (ε) %	Deformation speed mm/ sec	Strain rate ($\dot{\varepsilon}$), s^{-1}	Activation energy (Q), KJ/ mol	Forging temp., K	Ln- Z	Calculated γ- grain size, μm
1	8654.6	6272	27.53	300	6.15	366.105	1348	34.47	32.69
2	6272	4356	30.55	300	6.85	366.105	1313	35.45	29.85
3	4356	2898	33.47	300	7.86	366.105	1273	36.64	26.79
4	2898	1590	45.13	300	8.29	366.105	1223	38.10	23.63
5	1590	572	64.03	300	9.40	366.105	1213	38.53	22.84

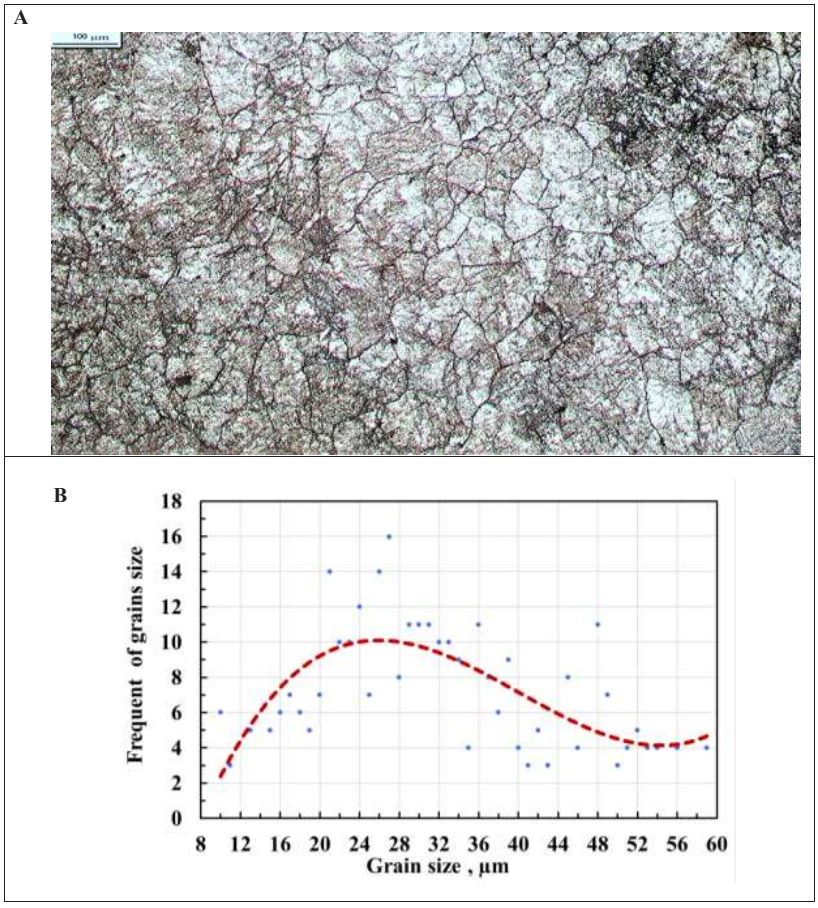

Fig. 12- Measured grain size of ferrite matrix generated after forging.
A- Forged microstructure, B- Grain size distribution of the ferrite matrix.

It is clear that, both strain (ε) and strain rate ($\dot{\varepsilon}$) increase, while the deformation temperature decreases from one step to the other. The current deformation parameters are leading to a continuous increase of the Z-parameter [15], while the expected γ- grain size would be successively refined [18], and reaches at the final 5^{th}-forging step to 22.84 μm.

Fig. 13 presents the numerically calculated Ln Z-parameter and expected γ- grain size for the 5 successive steps forging cycle. The forging cycle is leading to a repeated γ- grain refinement (Table I), which would transform to a matrix of fine α-grains after forging and air cooling, where the average measured grain size in Fig. 12, [18], was calculated as 32. μm.

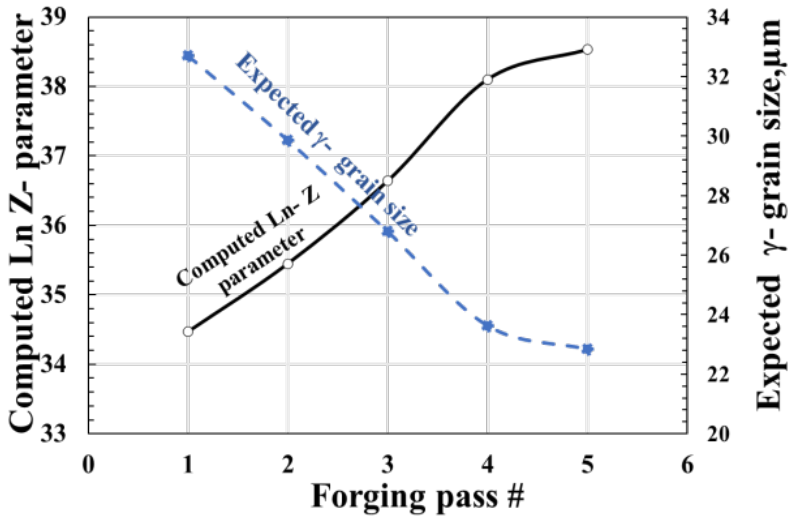

Fig. 13- value of computed Ln Z-parameter and expected γ- grain size for 5 successive steps forging cycle.

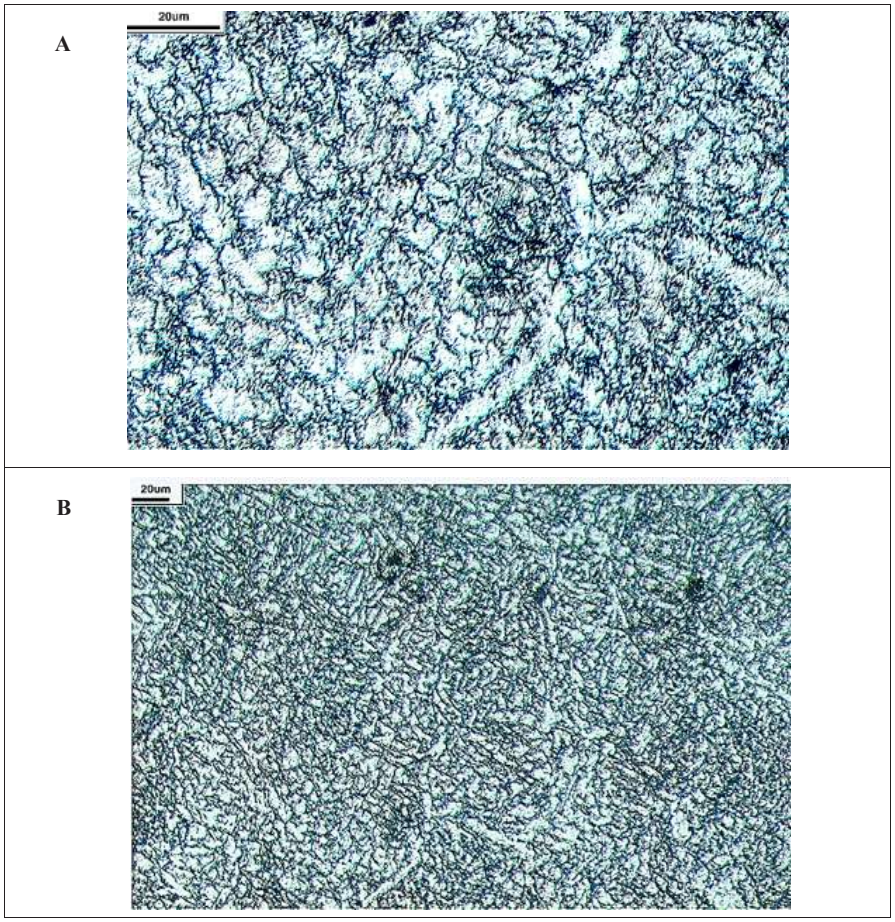

Fig. 14- Microstructure generated after a salt bath holding at 400 °C, followed by 2nd quenching either in oil (A) or in water (B).

Fig. 14 demonstrates the microstructure of both 2nd quenching in oil (A) and 2nd quenching in water (B) after salt bath 1st quenching at 400 °C. A ferrite matrix is more clearly presented in the oil quenching microstructure than that at the water quenching, due to lower cooling rate of oil rather than of water. Both of the 2nd quenching processes generate hard phases between the α-grains in the matrix. In case of oil 2nd quenching, a bainite phase is mostly generated, while martensite is favorably created by water 2nd quenching, where a higher cooling rate was prevailing.

For a more conformation, the scanning electron microscope (SEM) is extensively used for high magnifications and EDX qualitative analysis. Fig.15 presents generated microstructure after a 2nd quenching in oil bath at magnifications 8000X & 30000X respectively. 2nd quenching in oil after the salt bath holding generates bainite islands interspersing across freckled ferrite matrix with scattered Cr-Mo carbides.

Fig. 16 presents EDX qualitative chemical analysis of a bainite island generated by 2nd quenching in oil. The generated bainite phase contains mostly low carbon, which would be reflected positively on the ductility and toughness of the treated alloy.

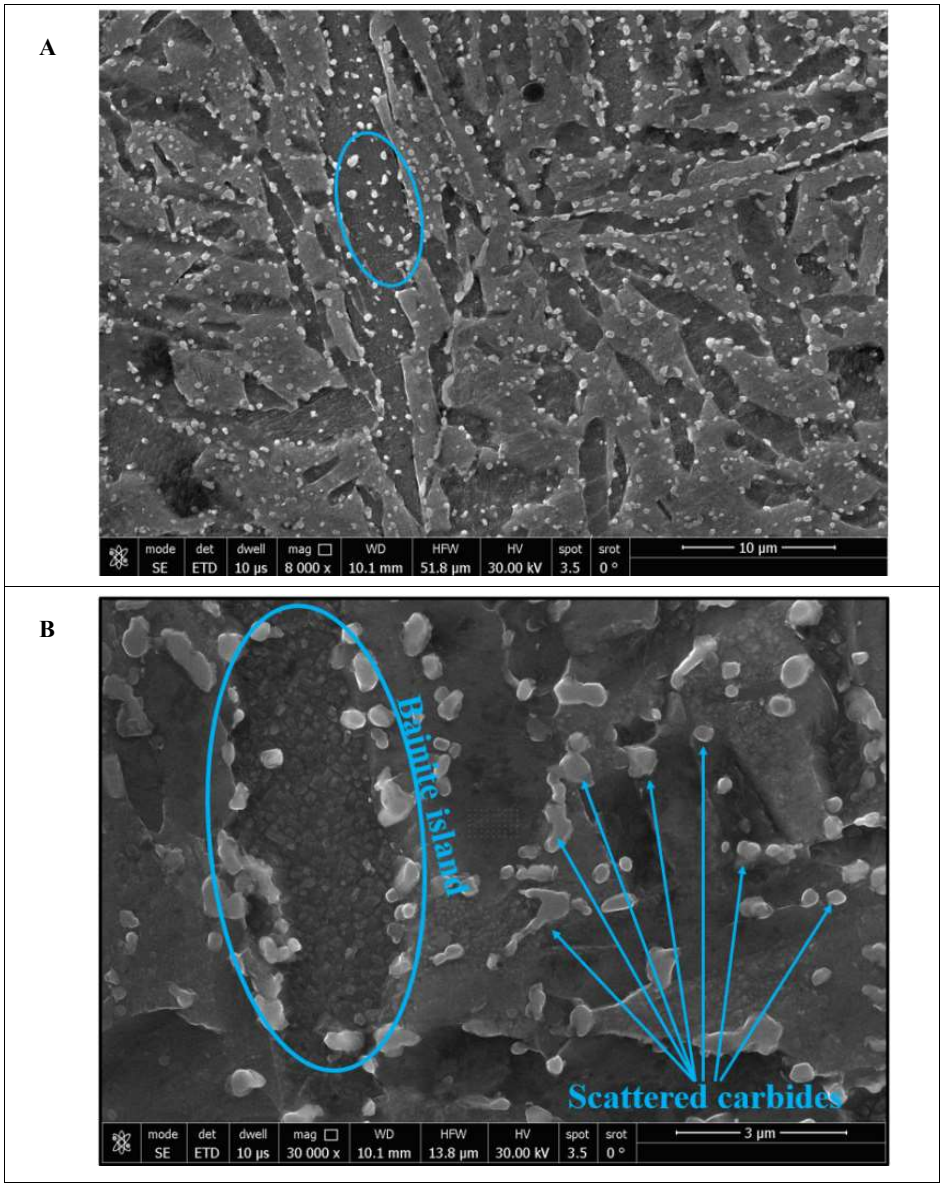

Fig. 15- Microstructure generated by a 2nd quenching in oil, containing bainite islands interspersing across freckled ferrite.

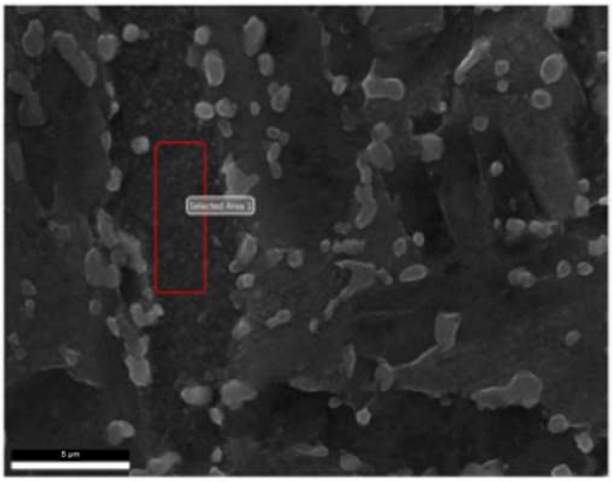

Element	Weight %	Atomic %	Error %
C K	0.71	3.2	81.9
SiK	2.76	5.3	13.55
CrK	10.61	11	3.59
MnK	0.76	0.75	26.57
FeK	79.07	76.33	1.85
MoK	6.09	3.42	38.51

Fig. 16- EDX qualitative chemical analysis of a bainite aggregate generated by 2nd quenching in oil.

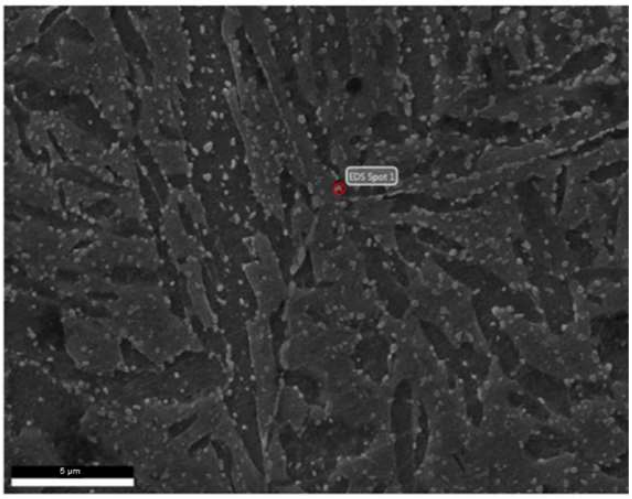

Element	Weight %	Atomic %	Error %
C K	3.38	14.02	21.21
SiK	2.42	4.29	14.02
CrK	13.27	12.72	3.24
MnK	0.9	0.81	22.09
FeK	71.24	63.59	2.01
MoK	8.79	4.57	28.77

Fig. 17- EDX qualitative chemical analysis of scattered Cr-Mo-carbides generated by 2nd quenching in oil.

On the other hand, Fig. 17 presents the EDX analysis of scattered Cr-Mo carbides, where the analysis contains high amounts of carbon, chromium and molybdenum confirming that the scattered dots are Cr, Mo-carbides as they are the most stable carbides at the working temperature range [4, 6]. The formation of $M_{23}C_6$ or M_6C carbides are controlled by relative contents of Cr and Mo in the carbide [5].

The previously bainitic aggregates generated at 400 °C are usually accompanied by retained austenite films [19]. Retained austenite, is originating from the residual austenite, which is not transformed into bainite at the end of the isothermal 400 °C holding [13]. 2nd quenching in water generates late martensite as a result of retained-austenite transformation [20]. Fig. 18 demonstrates widespread carbides existing between the ferrite matrix grains (A) and (micrograph B) presents the transformed platelet late martensite at a higher magnification (X 30000), which is generated at the temperature which reaches to Ms [20].

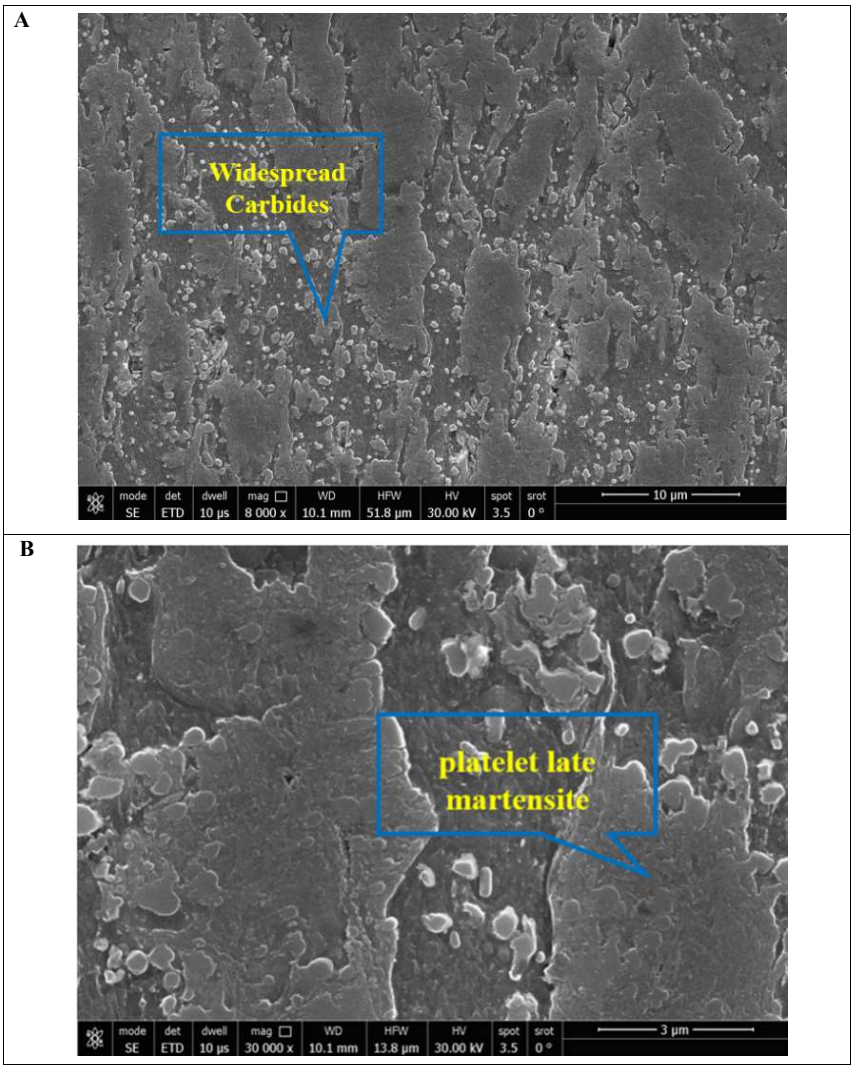

Fig. 18- Widespread carbides (A) that existing between the ferrite matrix grains integrated with transformed platelet late martensite (B).

4. Conclusion

The article is concerning with the development of valve steel alloy containing a blend of hard phases of bainite and mertensite due to processing with double fold cooling. Furthermore the structure contains excessive Cr-Mo stable carbides. It is concluded that;

1. Up to 1000 °C, the as-cast alloy structure contains both rich Cr-carbides as ($Cr_{23}C_6$) and rich Mo-carbides as (Mo_2C).
2. Forged microstructure composes mainly of ferrite, which are enveloped by a thin carbide layer.
3. On cooling after forging, γ- phase transforms to γ+α bi-phase region with precipitated Cr-Mo carbides as thin layered enveloping the ferrite grains and intersecting at the grains triple points with some other fine scattered carbides over the α-grains.
4. Both of the oil and water 2nd quenching processes generate hard phases integrating with the α-grains in the matrix. A low carbon - bainite phase islands accompanied by retained austenite films is mostly generated by oil 2nd quenching, while platelet late martensite is favorably created by water 2nd quenching.

Acknowledgment

The authors would like to sincerely thank EZZ Flat Steel in Ain Sokhna, Suez, for providing the raw steel material necessary to process multiple exhaust valve alloy trials, which significantly contributed to the completion of this study.

References

1. T. El-Bitar, M. E.-. Meligy and M. Khedr, "Investigation of Exhaust Valve Failure in a Marine Diesel Engine," Engineering Failure Analysis Journal, (2020);114: 104574.
2. M. Fonte, M. Freitas and L. Reis, "Failure analysis of a damaged diesel motor crankshaft," Engineering Failure Analysis, (2019); 102:1-6.
3. M. Avateffazeli, G. Webster, K. Tahmasbi and M. Haghshenas, "Very high cycle fatigue at elevated temperatures: A review on high temperature ultrasonic fatigue," Journal of Space Safety Engineering, (2022); 9:488-512.
4. "JMatPro commericial software, Version 15.0," November 2024.
5. X. Qin, X. Yan, D. Huang, X. Zhang, M. Qi and S. Yue, "Evolution Behavior of M23C6 Carbides Under Different Hot Deformation Conditions in Alloy 602 CA," Metals and Materials International, (2019); 25:1616–1625.
6. E. T. Turkdogan, "Physical chemistry of high temperature technology,"1st ed., Academic Press, 1980.
7. L. Mishnaevsky, "Computational Mesomechanics of Materials," Continuum Models and Discrete Systems, NATO Science Series In: Bergman, D.J., Inan, E. (eds). (2004); 158:123-128.
8. T. El-Bitar, A. Ismail, A. El-Morsy and A. Amer, "Deformation of Special Steels," Steel Grips, (2004); 2:364-371.
9. T. El-Bitar, M. El-Meligy and M. Gamil, "Development of X40CrSiMo10-2 steel series for heavy-duty in hot environment of marine diesel engines," Materials Research Proceedings, (2024); 44:374-380.
10. D. Pierce, A. Hayne, J. H. R. Graves, P. Maziasz, G. Muralidharan, A. Shyam, B. Wang, R. England and C. Daniel, "High temperature materials for heavy duty diesel engines: Historical and future trends," Progress in Materials Science, (2019);103:109-179.
11. T. El-Bitar, M. El-Meligy and M. Khedr, "Roll Pass design, numerical model and processing procedure of a 3rd generation dual phase sheet stee," Procedia Manufacturing, (2020); 50:173-178.
12. M. El-Meligy and T. El-Bitar, "Development of martensitic/bainitic rolled homogeneous bulletproof (RHBP) steel sheets for civilian applications," Advances in Materials and Processing Technologies, (2024); 10: 3595-3606.
13. L. Qian, Z. Li, T. Wang, D. Li, F. Zhang and J. Meng, "Roles of pre-formed martensite in below-Ms bainite formation, microstructure, strain partitioning and impact absorption energies of low-carbon bainitic steel," Journal of Materials Science & Technology, (2022);96:69-84.
14. Y. Wu, M. Zhang and X. Xu, "Investigations on hot deformation behaviors and abnormal variation mechanisms of flow stress at elevated temperature for X45CrSi93 valve steel," Journal of Materials Research, (2015); 30:1715–1726.
15. T. El-Bitar, M. El-Meligy, W. Borek and S. Ebied, "Grain Refinement Tracing of Dynamic and Metadynamic Recrystallization for a Penetrator Steel," Journal of Ultrafine Grained and Nanostructured Materials, (2024); 57:75-81.
16. H. L. Duan, X. M. Huang, H. C. Ji and Y. G. Li, "The Arrhenius constitutive model of steel 42CrMo for gear," Metallurgy, (2020); 59: 63-69.
17. H. D. Hongchao Ji, Y. Li, W. Li, X. Huang, W. Pei and Y. Lu, "Optimization the working parameters of as-forged 42CrMo steel by constitutive equation-dynamic recrystallization equation and processing maps," Journal of Materials Research and Technology, (2020);9:7210-7224.
18. H.-b. J. a, J.-m. Wang, Z.-y. Wang, Y. Li and X.-h. Cheng, "The effect of high-temperature ECAP on dynamic recrystallization behavior and material strength of 42CrMo steel," Materials Science and Engineering: A, (2023); 887:145732.
19. M. El-Meligy, T. El-Bitar and S. Ebied, "Creation of Fine Lath Martensite combined with Nano needle like Structured Carbides in Ultra high strength (UHS) Military Steels," Journal of Ultrafine Grained and Nanostructured Materials, (2023); 56:173-183.
20. K. Takashima, T. Nishimura, K. Yokoyama and Y. Funakawa, "Delayed Fracture Enhanced by Martensite Transformed from Retained Austenite in Ultra-high Strength Steel Sheet," ISIJ International, (2024) ;64:742-750.